Cement and Concrete Composites 106 (2020) 103462

Contents lists available at ScienceDirect

Cement and Concrete Composites

journal homepage: http://www.elsevier.com/locate/cemconcomp

Thermal behavior of alkali-activated fly ash/slag with the addition of an aerogel as an aggregate replacement

Joonho Seo [a], S.J. Bae [a], D.I. Jang [a], Solmoi Park [a], Beomjoo Yang [b], H.K. Lee [a,*]

[a] Department of Civil and Environmental Engineering, Korea Advanced Institute of Science and Technology (KAIST), 291 Daehak-ro, Yuseong-gu, Daejeon, 34141, Republic of Korea
[b] School of Civil Engineering, Chungbuk National University, 1 Chungdae-ro, Seowon-gu, Cheongju, Chungbuk, 28644, Republic of Korea

ARTICLE INFO

Keywords:
Alkali-activated material
Fly ash
Slag
Aerogel
High temperature
Characterization

ABSTRACT

The present study investigated the thermal behavior of alkali-activated fly ash/slag with the addition of an aerogel as an aggregate replacement. Samples having aggregate-to-aerogel replacement ratios of 25, 50, and 75% by volume were fabricated and were exposed to temperatures of 200 °C, 400 °C, 600 °C or 800 °C. Water contact angle and thermal conductivity tests were carried out to assess the dispersion of the aerogel in an alkaline environment. X-ray diffractometry, mercury intrusion porosimetry, compressive strength test and thermogravimetry were conducted to investigate the thermal evolution of the reaction products, the pore structures and the mechanical strength. The results revealed that the incorporated aerogel mitigated thermal expansion up to 600 °C while also inducing rapid thermal shrinkage above 600 °C. Meanwhile, the pore structures of the samples with high aerogel contents were scarcely altered upon exposure to high temperatures, showing a level similar to those observed at 25 °C.

1. Introduction

The significant CO_2 emissions associated with the manufacture of Portland cement clinkers have necessitated the development of alkali-activated materials [1,2]. The practical use of alkali-activated materials is of paramount importance with regard to the conservation of natural resources and the production of highly durable construction materials [3]. Several decades have witnessed active discussions focusing on experimental findings related to the physicochemical properties of alkali-activated materials, ultimately toward greater openness with regard to relevant fields and to the public [2,4]. As a result of these attempts, alkali-activated materials are now seriously considered to have potential in the quest to realize a sustainable and alternative cementing system [1,2,4]. Alkali-activated materials can typically be manufactured by the alkaline activation of various aluminosilicate precursors, such as fly ash, metakaolin, red mud and blast furnace slag [5,6]. There have been consistent attempts to investigate alkali-activated materials to meet the particular requirements of building members in a manner similar to how Portland cement does so [7]. Current applications of alkali-activated materials include the production of precast structural members, different types of grout, masonry bricks, aerated concrete, heat-resistant concrete and matrixes for the solidification and immobilization of extremely hazardous or radioactive waste. These areas are also anticipated to expand in the future [7,8].

In recent years, silica aerogels have been highlighted due to their unique air-filled structures [9]. A silica aerogel is a siliceous substance that consists of a network of interconnected nanostructures [10]. More than 90% of a typical silica aerogel consists of air voids with a particle size of less than 50 μm. These particles lead to the formation of a high surface area, imparting in this material low solid conductivity and thermal energy diffusivity [9,11]. These inherent properties allow the aerogel to exhibit various useful characteristics, such as outstanding thermal insulation (thermal conductivity as low as 17–22 mW/mK), high hydrophobicity with a water contact angle value exceeding 150°, a high surface area (600–800 m^2/g) and high porosity (>90%) [12–17]. Furthermore, silica aerogels maintain their thermo-stability upon exposure up to 540 °C and are converted into hydrophilic aerogels [18]. These versatile properties of silica aerogels have been drawing attention in relation to many possible practical applications, such as thermal insulation [12,13,19], chemical sensors [14,15] and flame retardants [16,17].

Many attempts have been made to utilize aerogels as an aggregate replacement component in cementitious materials in order to produce cementitious composites with low thermal conductivity levels. Gao et al.

* Corresponding author.
E-mail address: haengki@kaist.ac.kr (H.K. Lee).

https://doi.org/10.1016/j.cemconcomp.2019.103462
Received 18 July 2019; Received in revised form 4 October 2019; Accepted 14 November 2019
Available online 18 November 2019

carried out an experimental study of lightweight and thermally insulating Portland cement concrete prepared by replacing the aggregate in the concrete with an aerogel and fabricated concrete samples with a density level of 1,000 kg/m^3, thermal conductivity of 0.26 W/mK and a compressive strength of 8.3 MPa at an entire aggregate replacement ratio [20]. Furthermore, Gao et al. observed that the incorporated aerogel in their study remained stable during cement hydration [20]. Ng et al. produced aerogel-incorporated mortar samples with low water-to-cement ratios, concluding that the incorporation of the aerogel led to a significant strength loss, whereas the reduction in the thermal conductivity was not noticeable considering the high aerogel replacement level (as high as 80 vol. %) [21]. Another study conducted by Ng et al. produced aerogel-incorporated ultra-high-performance concrete with thermal conductivity as low as 0.1 W/mK, indicating the potential to develop high-strength concrete with a significantly low thermal conductivity value [22]. Júlio et al. synthesized an inorganic silica-based aerogel and manufactured cementitious renders with thermal conductivity of 0.567 W/mK and a density of 1,450 kg/m^3 with the aid of an anionic surfactant [23]. Júlio et al. also demonstrated fair stability of the synthetic aerogel in a pore solution of cement paste with no effects on the inner structure of the hydration products [23].

A study performed by Huang et al. [24] prepared lightweight aerogel-geopolymer composites having a bulk density of 306.5 g/cm^3 and thermal conductivity of 0.048 W/mK via a sol-gel immersion method. However, the mechanical strength of the samples presented in Huang et al. [24] was insufficient for the samples to be used as a construction material. Despite several studies of the use of aerogels in cementitious materials, investigations of the thermal properties of alkali-activated materials with the addition of an aerogel as an aggregate replacement are well beyond our current knowledge. In particualr, recent studies are focusing on the chemistry of alkali-activated materiarls with a blend of slag and aluminosilicates (e.g., fly ash and metakaolin) [5,45,46], which possess a potential of omitting high-temperature curing process [47]. Furthermore, the physicochemical properties of the alkali-activated blended materials exposed to elevated temperatures have been actively investigated [28,48,49]. Nevertheless, a detailed examination of the use and role of aerogel in alkali-activated blended materials at high temperatures is not available. The present study investigated the thermal characteristics of alkali-activated fly ash/slag samples with various aerogel replacement ratios. The dispersion of the aerogel in the matrix was examined by means of water contact angle tests and thermal conductivity tests. Dilatometry test were carried out to investigate the volumetric stability at elevated temperatures. In addition, the samples were exposed to 25 °C, 200 °C, 400 °C, 600 °C or 800 °C to evaluate their thermal behavior at high temperatures. The present study experimentally focused on the thermal evolution of the reaction products, the pore structure, and the compressive strength development of alkali-activated fly ash/slag with the addition of an aerogel as an aggregate material.

2. Experimental program

2.1. Materials and sample preparation

Fly ash, classified as class F in accordance with ASTM C618 [25], and blast furnace slag were used as the binder materials. Standard sand (Joomoonjin Silica Sand Co., Ltd.) with a density level of 1,450 kg/m^3 and an aerogel (Jiosaerogel Corp.) with a particle size in the range of 40–50 μm and a density level of 96.7 kg/m^3 were used as aggregates. The posity, surface area, and average pore diameter of the aerogel powder, as provided by the manufacturer, were >95%, 665.7 m^2/g, and 3.59 nm, respectively. The chemical composition as obtained by the X-ray fluorescence analysis and X-ray diffraction (XRD) pattern of the raw materials are provided in Table 1 and Fig. 1, respectively. The aerogel is primarily composed of SiO_2 with an amorphous structure, as evidenced by a hump-like feature centered at around 20° 2θ in the XRD pattern. The particle size distribution of the raw materials is presented in Fig. 2. A mixture of a 4 M sodium hydroxide solution and a liquid water glass (sodium silicate solution, Korean Industrial Standards KS grade 3; SiO_2 = 29 wt. %, Na_2O = 10 wt. %, H_2O = 61 wt. % and specific gravity = 1.38) at a weight ratio of 2 to 1 was used as an alkali-activator.

Samples were synthesized by the alkaline activation of the fly ash and slag blends and by replacing the sand with the aerogel at 0, 25, 50 and 75 vol. %. The mixture proportions of the samples are tabulated in Table 2. Note that the activator-to-binder ratio and the binder-to-aggregate ratio of the samples were kept constant at 0.5 by weight ratio and 0.4 by volume ratio, respectively, and that the sample ID denotes the volume fraction of the aerogel as an aggregate. Mortar samples with 100 vol. % replacement of the sand with aerogel (namely A100) were not prepared in this study since they were not able to achieve proper workability. The powder and liquid were mechanically mixed for 10 min and poured into a cubical mold having dimensions of 50 × 50 × 50 mm^3. For chemical analyses and dilatometry test, sand was excluded in the identical mixture proportion used for fabricating the mortar samples to exclude the undesired effect of sand. Samples were demolded after one day of initial curing and were further cured in a curing chamber for 27 days at 25 °C and R.H. 50%, which fairly resemble the average ambient condition. After 28 days of curing, the samples were exposed to a temperature of 200 °C, 400 °C, 600 °C or 800 °C at a constant heating rate of 10 °C/min using an electric furnace. The samples were dried at 50 °C for one day beforehand to remove any capillary water, thereby eliminating any potential of spalling at the high temperatures [26–28]. The designated temperatures were maintained for 2 h in order for the samples to reach a state of thermal equilibrium [26–28]. Shortly afterward, the samples were allowed to cool down naturally to 25 °C inside the electric furnace. After exposure to a high temperature, the samples without sand were immersed in an acetone solution and vacuum dried for 24 h to halt any further reaction. Thereafter, the samples were manually ground to pass a 75 μm sieve for XRD and thermogravimetric analysis (TGA), while fractured sample were used for the mercury intrusion porosimetry (MIP). Mortar samples were used for the water contact angle test, thermal conductivity measurement and compressive strength test. Noting that the samples for the dilatometry test were dried at 50 °C for two days before testing so as to prevent the testing device from being damaged due to spalling and/or from excessive movement during the initial measurement, mainly due to the dissipation of free water [29]. Sand was excluded from the dilatometry tests because the volumetric change of the samples can be governed significantly by the rapid thermal expansion of the sand [30].

2.2. Test methods

The thermal characteristics of the aerogel-incorporated alkali-activated fly ash/slag were explored by means of various analytical techniques. Water contact angle test, thermal conductivity measurement, dilatometry, XRD, MIP and unconfined compressive strength test were performed. Cubical samples with dimensions of 50 × 50 × 50 mm^3 were used for the water contact angle test, thermal conductivity measurement and compressive strength test while parallelepiped samples with dimensions of 10 × 10 × 5 mm^3 were used for the dilatometry test. The sample dimension for the dilatometry test was chosen in accordance with the requirements of the testing device and such sample dimension allowed the samples to easily reach the thermal equilibrium state of the entire sample. It should, however, be noted that the dilatometry test result of samples having larger dimension than those used in this study may differ due to temperature gradient in the samples TGA was carried out to evaluate the reaction products quantitatively.

The water contact angle test was carried out using a PHOENIX-300 TOUCH instrument (S-EO). The moment of contact was captured under an identical condition for all samples. Thermal conductivity was measured using a TPS 2500 S Hot Disk AB device (Gothenburg) in accordance with ISO standard 22007-2. The thermal conductivity value

Table 1
Chemical composition of the raw materials used in this study.

(wt. %)	CaO	SiO_2	Al_2O_3	Fe_2O_3	SO_3	MgO	K_2O	Na_2O	LOI[a]
Fly ash	3.4	63.9	19.4	3.8	0.4	1.4	0.6	0.3	4.8
Slag	43.7	36.4	14.3	0.3	0.1	3.5	0.5	0.2	1.0
Aerogel	–	99.6	–	–	–	–	–	–	0.4

[a] Loss-on-ignition.

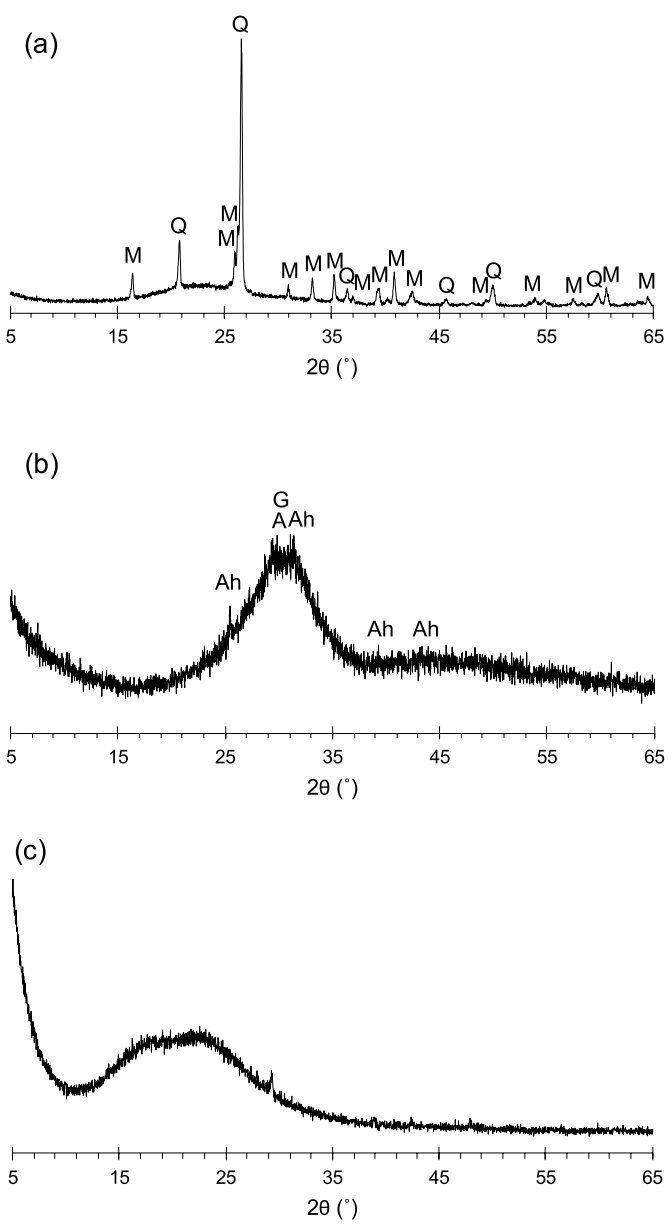

Fig. 1. XRD pattern of the (a) fly ash, (b) slag and (c) aerogel used in this study. The annotations are as follows: M-mullite, Q-quartz, Ah-anhydrite, G-gehlenite and A- åkermanite.

of the samples were averaged from three replicas. Dilatometry was measured using a TMA Q400 device (TA Instruments). Samples were heated at a constant heating rate of 5 °C/sec under a constant vertical force of 0.05 N. The horizontal deformation of the samples in the temperature range of 25–800 °C was recorded. XRD was conducted using an EMPYREAN device (Malvern Panalytical) with CuKα radiation at a generator voltage and tube current of 40 kV and 30 mA, respectively. XRD patterns of the samples were collected by scanning the samples on a

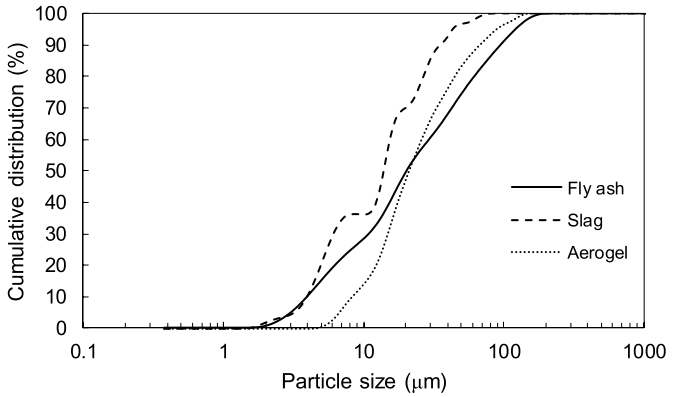

Fig. 2. Particle size distribution of the raw materials used in this study.

Table 2
Mixture proportion of aerogel-incorporated alkali-activated fly ash/slag mortar expressed as the mass ratio.

Sample ID	Binder (wt. %)		Aggregate (wt. %)		Aerogel out of total weight (wt. %)	Aerogel out of total volume (vol. %)
	Fly ash	Slag	Sand	Aerogel		
A0	5	5	14.60	0	0	0
A25	5	5	10.95	0.24	0.93	17.86
A50	5	5	7.30	0.48	2.08	35.61
A75	5	5	3.65	0.73	3.66	53.52

rotating stage at 5–65° 2θ with a step size of 0.026° 2θ and at 1.56 s per step. MIP was carried out using an AutoPore IV 9500 device (Micromeritics). The pressure for the MIP analysis ranged from 0.1 to 61,000 psi (from 0.00069 to 420.6 MPa). The unconfined compressive strength was measured using a 2,500 kN compression testing device (INSTRON) at a constant loading rate of 0.02 mm/s. Three cubical samples were tested to assess the average compressive strength. The TGA was performed using a Labsys Evo TG-DTA instrument (SETARAM). N_2 gas was injected into the furnace of the TG instrument to prevent the samples from oxidation during the measurement process. 5.5–6.0 mg of the sieved samples were used for the TGA. Relative weight variations of the samples were recorded in the temperature range of 25–1000 °C.

3. Results

3.1. Water contact angle

The water contact angle of the aerogel-incorporated alkali-activated fly ash/slag mortar after 28 days of curing is displayed in Fig. 3. Measurement of the water contact angle is a particularly useful technique for determining the degree of hydrophobicity of cementitious composites. As is widely postulated, higher hydrophobicity of a composite leads to a higher water contact angle [31]. The water contact angle value of the samples showed proportionality with an increase in the aerogel content, i.e., 18.84°, 25.58°, 27.03° and 29.69° for the A0, A25, A50 and A75 samples, respectively. The A75 sample showed a higher water contact angle value by 141.77% compared to the A0 sample. Such notable

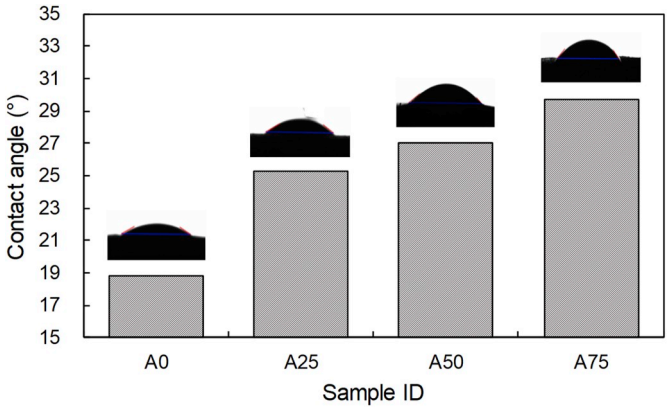

Fig. 3. Water contact angle of the aerogel-incorporated alkali-activated fly ash/slag mortar.

differences in the water contact angle value of the samples are clearly due to the fact that the hydrophobic aerogel was well dispersed in the matrix.

3.2. Thermal conductivity

The thermal conductivity of the aerogel-incorporated alkali-activated fly ash/slag mortar after 28 days of curing is shown in Fig. 4. The thermal conductivity values of the A0, A25, A50 and A75 samples were 1.8, 1.3, 1.1 and 0.9 W/mK, respectively, showing inverse proportionality with an increase in the aerogel content. The A75 sample showed the lowest thermal conductivity of approximately 50% of that measured for the A0 sample. This observation implies that the incorporated aerogel was properly dispersed, thereby leading to the formation of a highly porous structure. The clear effect of aerogel incorporation on the decrease in the thermal conductivity is in fair agreement with the experimental findings of earlier works [20–22]. Note that the samples for the thermal conductivity measurement were not fully dried before testing, meaning that the remnant capillary water may affect the results [43,44], yet the differences in the obtained values are clear enough to be compared with each other.

3.3. Dilatometry

The dilatometry of the aerogel-incorporated alkali-activated fly ash/slag after 28 days of curing is displayed in Fig. 5. Notable thermal movements occurred mainly in three regions: 250 °C – 500 °C, 500 °C – 600 °C and above 600 °C. It should be noted that the samples for the dilatometry test were dried in an oven beforehand to evaporate free and weakly bound water. Therefore, the volumetric movements by water

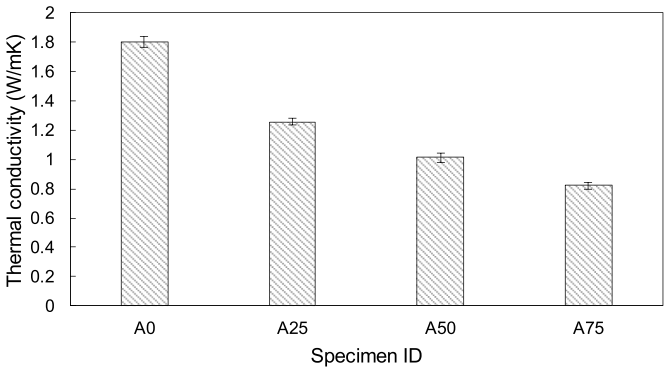

Fig. 4. Thermal conductivity of the aerogel-incorporated alkali-activated fly ash/slag mortar.

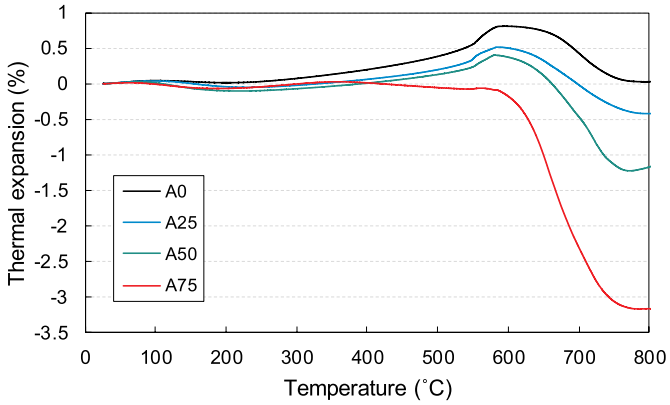

Fig. 5. Dilatometry of the aerogel-incorporated alkali-activated fly ash/slag.

loss (typically occurring between 25 °C – 100 °C) in the samples were not recorded in this study. The expansion in the first region is associated with the physically and chemically bound water in the geopolymers, which can be referred to as the interstitial water and the water loss from dehydroxylation, respectively [29,32]. The A0 sample exhibited the most prominent expansion in this region, while the volumetric movement of the A75 sample was barely observable. This is likely attributed to the difference among the pore structures of the samples [33]. An abrupt and sharp expansion identified in the second region is attributed to the thermal transformation of quartz α phase into β phase in fly ash, which occurs at around 570 °C [34,35]. It is interesting to note that the A75 sample showed relatively minor thermal expansion in the second region. The third region, which contains remarkable shrinkage, corresponds to the glass transition temperature [34]. The reaction products and pore structure of the samples collapse at the glass transition temperature, at which the Al-incorporated Si tetrahedral interconnected framework undergoes softening and a sintering-induced viscous flow commences [34,36]. The rapid shrinkage featured in this temperature region due to sintering subsequently led to recrystallization and densification of the samples [37]. The samples with the aerogel showed much better volumetric stability up to 600 °C compared to the A0 sample. Nevertheless, aerogel incorporation resulted in severe shrinkage above 600 °C.

3.4. XRD

The XRD patterns of the aerogel-incorporated alkali-activated fly ash/slag samples exposed to high temperatures are shown in Fig. 6. The main reaction product of the samples at 25 °C was C–S–H (typically referred to as C-(A)-S-H), in which Si is partially substituted with Al [50]. Crystalline phases from the raw fly ash, i.e., quartz (SiO_2, PDF #00-046-1045) and mullite ($Al_{4.44}Si_{1.56}O_{9.78}$, PDF# 01-074-4143), persisted in all samples. The crystalline phases featured in the patterns were unaltered upon exposure to 600 °C. Meanwhile, a noticeable reduction in the peak intensity corresponding to the presence of C-(A)-S-H was observed. The hump-like shape of the C-(A)-S-H, due to its inherent amorphous nature, was scarcely identified in the samples exposed to a temperature of 600 °C, signifying that the thermal decomposition of the C-(A)-S-H in the alkali-activated fly ash/slag occurred at a temperature between 400 °C and 600 °C.

Upon exposure to a temperature of 800 °C, the samples showed dramatic changes in their patterns regardless of the aerogel content. The patterns displayed peaks corresponding to the presence of åkermanite ($Ca_2MgSi_2O_7$, PDF #01-074-0990) and gehlenite (Ca_2AlSiO_7, PDF #00-035-0755), which were identifiable in the raw slag, implying that crystallization occurred in the samples exposed to the 800 °C. Other than these findings, the presence of anorthite ($CaAl_2Si_2O_8$, PDF #01-070-0287), nepheline ($NaAlSiO_4$, PDF #01-088-1231) and wollastonite

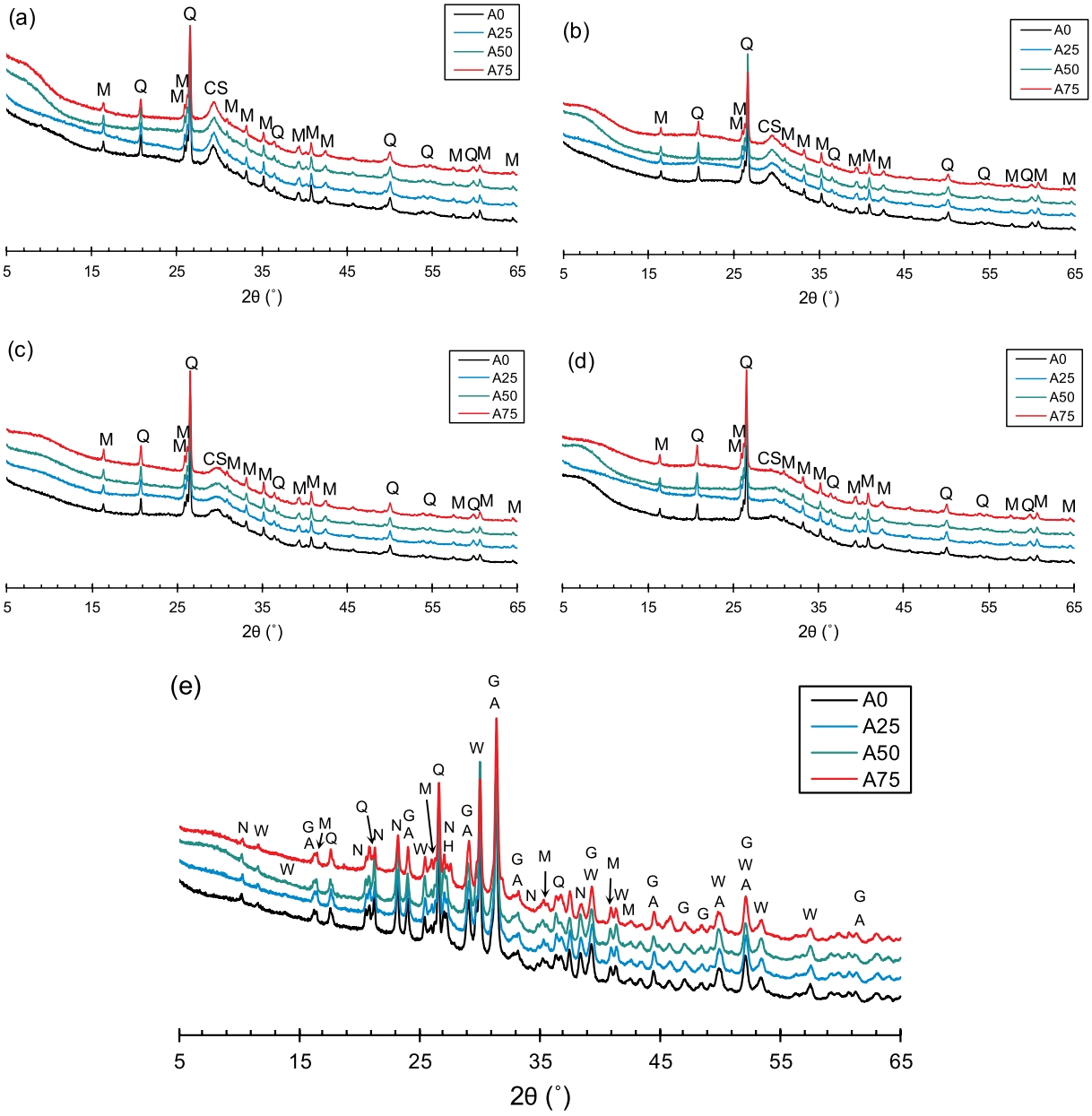

Fig. 6. XRD pattern of aerogel-incorporated alkali-activated fly ash/slag exposed to (a) 25 °C, (b) 200 °C, (c) 400 °C, (d) 600 °C and (e) 800 °C. The annotations are as follows: M-mullite, Q-quartz, CS- C-S-H, W- wollastonite, N- nepheline, G-gehlenite, An-anorthite and A- åkermanite.

($Ca_3Si_3O_9$, PDF #01-076-1846) was observed, in close agreement with earlier findings [28]. These crystals are typically found in aluminosilicate minerals exposed to high temperatures [28,34]. Meanwhile, aerogel incorporation did not lead to a noticeable difference in any of the patterns [38].

3.5. MIP

The MIP test results of the aerogel-incorporated alkali-activated fly ash/slag samples exposed to high temperatures are illustrated in Fig. 7. The samples tested at 25 °C showed a pores with diameters of less than 10 nm, which can be categorized as gel pores [28,39]. The samples with the aerogel displayed bimodal aspects in the form of a secondary peak which appeared in larger pore sizes as the aerogel content was increased. Upon exposure to the 200 °C, gel pores were diminished, and this aspect persisted up to 400 °C. All samples exposed to the temperature of 600 °C exhibited a significant amount of pores with diameters between 10 nm and 20 nm, in close agreement with results reported by Park et al. [28]. Pores with diameters of less than 100 nm were no longer identifiable in the samples exposed to 800 °C. It should be noted that the pores with diameters between 1,000 and 50,000 nm were not altered in the samples dosed with the aerogel, indicating that the formation of a very porous skeleton induced by the incorporation of the aerogel was not affected by aerogel high temperatures.

3.6. Compressive strength

The compressive strength of the aerogel-incorporated alkali-activated fly ash/slag mortar samples exposed to high temperatures is shown in Fig. 8. The incorporated aerogel significantly affected the compressive strength of the samples, as indicated by the strength values at 25 °C. The compressive strength of the A0 sample decreased rapidly after reaching its highest strength level at 200 °C, while the samples with the aerogel showed much less strength alteration with an increase in the

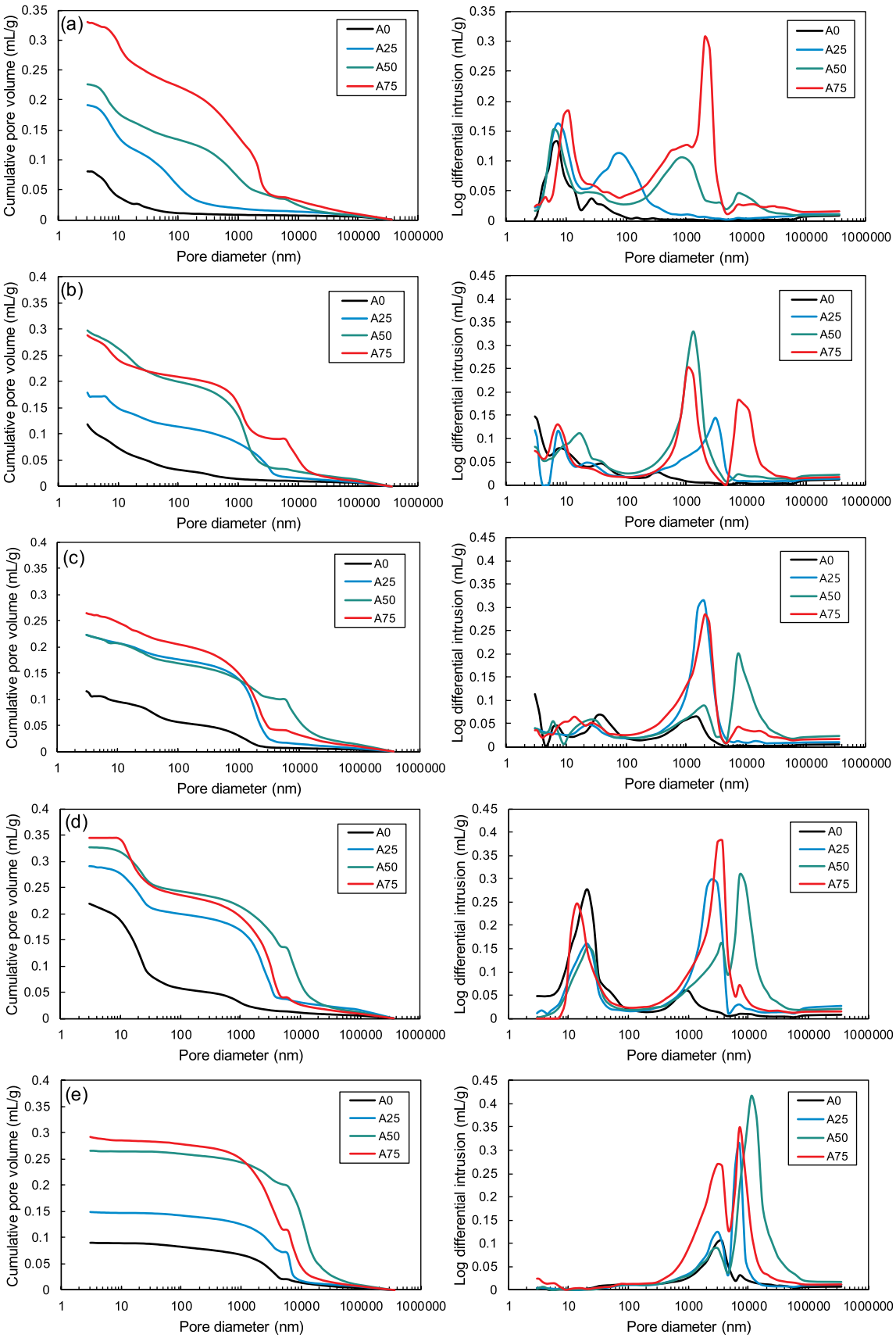

Fig. 7. MIP test result of aerogel-incorporated alkali-activated fly ash/slag exposed to (a) 25 °C, (b) 200 °C, (c) 400 °C, (d) 600 °C and (e) 800 °C.

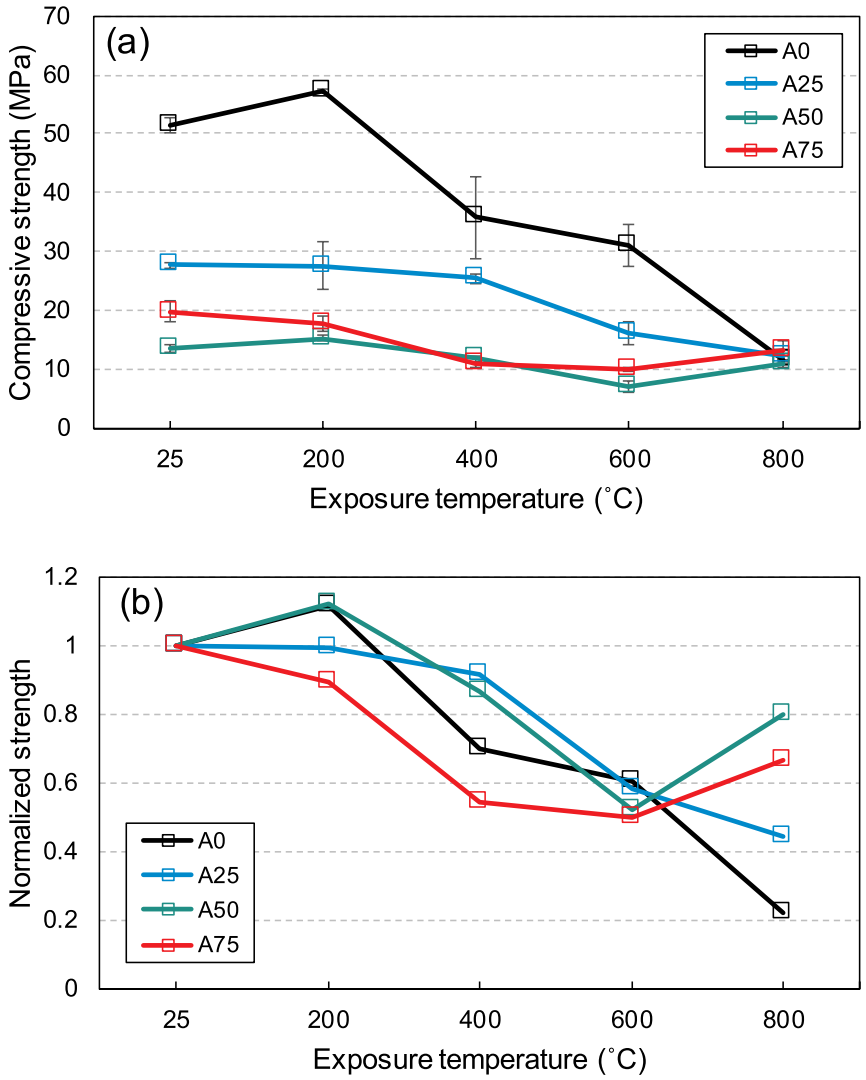

Fig. 8. (a) Compressive strength and (b) normalized compressive strength of aerogel-incorporated alkali-activated fly ash/slag mortar exposed to high temperatures.

temperature. The normalized compressive strength of the samples with respect to that measured at 25 °C is displayed in Fig. 8 (b). The samples with the aerogel showed noticeable residual strength even after exposure to 800 °C, maintaining 40–80% of their initial strength, while the A0 sample exhibited a drastic loss of strength with an increase in the temperature.

4. Discussion

Aerogel incorporation in cement-based materials generally induces the formation of a highly porous inner matrix whereby one can fabricate lightweight materials with low thermal conductivity [20–24,38]. Analogous aspects were observed in the alkali-activated fly ash/slag here with the addition of an aerogel as an aggregate replacement. The compressive strength and thermal conductivity of the samples with the aerogel were significantly reduced. Similar strength reductions can be found in the literature due to the inherent properties of the incorporated aerogel [40,41]. In addition, water contact angle test results proved that the samples with higher aerogel contents showed higher hydrophobicity, meaning that the aerogel can properly be dispersed in an alkaline environment. Furthermore, TGA results quantitatively demonstrated that the relative weight loss of the samples in the temperature region of 25–650 °C showed similar values with different incorporated aerogel contents (Table 3), in which this temperature region includes the weight loss corresponding to dissipation of bound water, decomposition of the reaction products, and the polycondensation of silanol and/or aluminol groups on the surface of the geopolymers [42]. This was partially reflected in the pore size distribution curves, which showed notable and unchanged pore populations corresponding to the presence of an aerogel, implying that the incorporated aerogel did not take part in the reaction.

The porosity and bulk density of the aerogel-incorporated alkali-activated fly ash/slag exposed to high temperatures are shown in Fig. 9. The samples showed no particular trend in the porosity upon exposure to a temperature of 400 °C. Thereafter, the samples reached their highest porosity at 600 °C and then showed a rapid reduction at 800 °C, while the bulk density of the samples exhibited an opposite trend. The radical alteration featured at 800 °C is associated with the recrystallization of the reaction products in the samples, as indicated by the XRD results.

Table 3
Relative weight loss (%) of aerogel-incorporated alkali-activated fly ash/slag in the temperature region of 25–650 °C.

Sample ID	A0	A25	A50	A75
Weight loss (%)	10.29	10.22	9.94	11.89

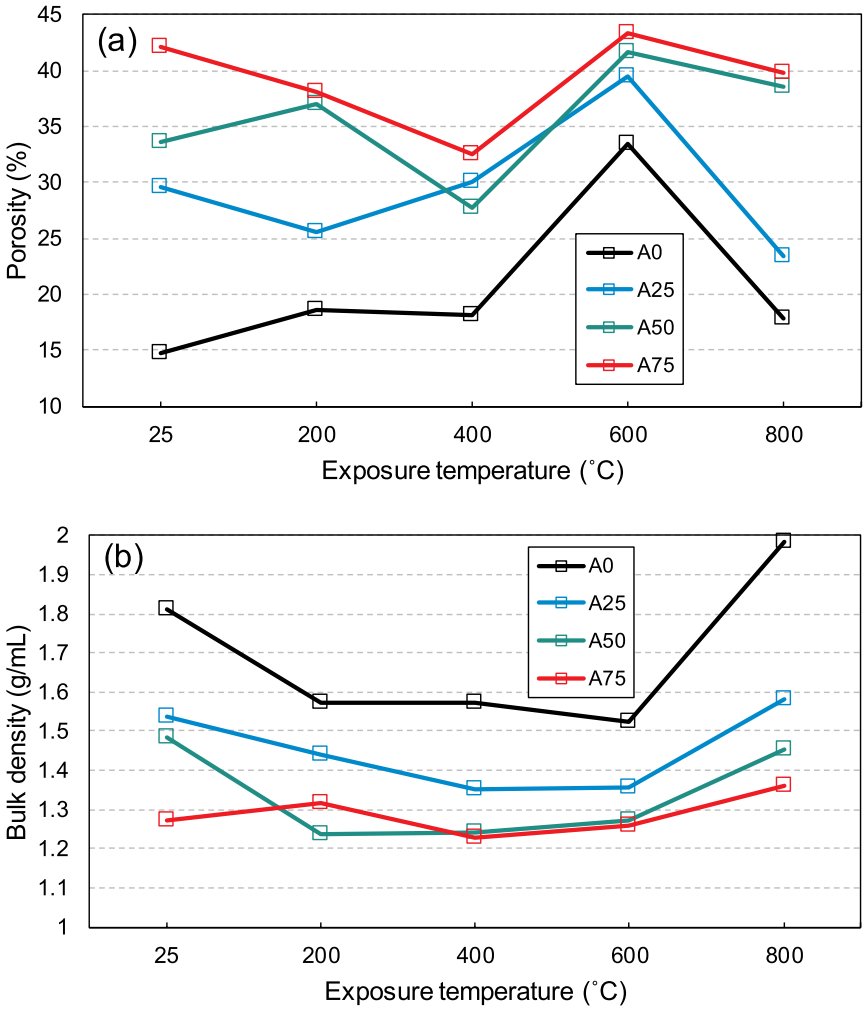

Fig. 9. (a) Porosity and (b) bulk density of aerogel-incorporated alkali-activated fly ash/slag exposed to high temperatures.

However, the extent of this was vastly mitigated by aerogel incorporation; i.e., the porosity and bulk density values of the A75 sample at 600 °C and 800 °C showed similar levels and were nearly identical to those at 25 °C, signifying that the incorporated aerogel buffered the volumetric thermal degradation of the global matrix. In addition, the dilatometry test results of the samples with the aerogel showed fair volumetric stability upon exposure to the 600 °C. These aspects indicate the potential of the practical applicability of the aerogel as an extremely low-heat-deformable material.

Cementitious renders at high temperatures inevitably demonstrate incompatibility between the aggregates and the paste (typically displays initial signs in the temperature region of 200 °C – 300 °C) due to the severe thermal expansion of the sand and/or gravel, which ultimately results in a significant reduction of the mechanical strength [30]. In this regard, the use of an aerogel as an aggregate replacement can alleviate the volumetric instability. As revealed via the dilatometry test here, thermal expansion of the samples was reduced with an increase in the aerogel content upon exposure from 25 °C to 600 °C, in which typical mortar and concrete undergo rapid thermal expansion in this temperature region in addition to that caused by the reaction products. Furthermore, the abrupt thermal shrinkage that occurred at the sintering point was higher in the samples with a higher aerogel content, which can be considered to compensate for the thermal expansion of the aggregate properly at temperatures above 600 °C. This was evidenced by the compressive strength test results, which illustrated that the A50 and A75 samples exposed to high temperatures showed nearly unaltered strength levels compared to that measured at 25 °C due to fact that the aerogel reduced the thermal deformation of the mortar samples used in this study.

It was noted in a previous study that a large number of pores in the matrix can ease the capillary tensile force which arises during the evaporation of chemically bound water [32], in close agreement with the results presented in this study. Meanwhile, the reaction products formed during the alkaline activation of the precursors (i.e., fly ash and slag) were converted into new phases by calcination, which can influence the thermal stability of the samples above the sintering temperature [29]. As observed in the XRD patterns, calcination induced the formation of new crystalline products of wollastonite, nepheline and gehlenite, which are known to display thermal stability [29]. Moreover, unreacted fly ash embedded in the samples can act as a filler, thereby restraining thermal shrinkage and cracking [32]. It is clear that these aspects relieved the thermal shrinkage of the A0 sample above the sintering temperature. However, samples with higher aerogel contents showed greater thermal shrinkage above the sintering temperature, indicating that the thermally stable aerogel affected the restraining phenomenon which typically occurs in geopolymers.

5. Concluding remarks

The present study investigated the thermal behavior of alkali-

activated fly ash/slag with the addition of an aerogel as an aggregate replacement. Microstructural evolution and thermal characteristics of the samples with different aerogel replacement levels were explored either at ambient temperature or at high temperatures of up to 800 °C. The key findings obtained from this study are summarized below.

(1) The water contact angle and thermal conductivity tests indicated that the incorporated aerogel was properly dispersed in the alkali-activated fly ash/slag and significantly reduced the thermal conductivity.
(2) Aerogel incorporation did not induce differences in the phase assemblages or in the amounts of the reaction product, meaning that the aerogel did not take part in the alkaline activation of the precursors.
(3) Aerogel incorporation greatly mitigated the thermal modification of the porosity and bulk density values, outcomes closely associated with the strength development of the samples with high aerogel contents tested at high temperatures.
(4) The samples with a high aerogel content displayed no thermal movement upon exposure to 600 °C, though the samples showed rapid thermal shrinkage afterward.

Declaration of competing interest

There are no conflicts to declare.

Acknowledgments

This study was supported by the National Research Foundation of Korea (NRF) of Korean government (Ministry of Science & ICT) [Grant Number: 2017R1A5A1014883] through Smart Submerged Floating Tunnel System Research Center. The authors acknowledge the use of Thermal Analysis System at the Korea Basic Science Busan Center, and would like to thank Dr. H.G. Kim for assistance with Thermal Analysis System. The authors also acknowledge the use of Particle and Pore size Analysis System at the Korea Basic Science Jeonju Center, and would like to thank Dr. S.J. Lee for assistance with Particle and Pore size Analysis System.

References

[1] J.L. Provis, S.A. Bernal, Geopolymers and related alkali-activated materials, Annu. Rev. Mater. Res. 44 (2014) 299–327.
[2] J.L. Provis, A. Palomo, C. Shi, Advances in understanding alkali-activated materials, Cement Concr. Res. 78 (2015) 110–125.
[3] C. Shi, J. Qian, High performance cementing materials from industrial slags – a review, Resour. Conserv. Recycl. 29 (2000) 195–207.
[4] J.L. Provis, J.S. Van Deventer, Alkali-activated Materials: State-Of-The-Art Report, Springer Science & Business Media, 2013. Rilem TC 224-AAM 13.
[5] N.K. Lee, H.K. Lee, Reactivity and reaction products of alkali-activated, fly ash/slag paste, Constr. Build. Mater. 81 (2015) 303–312.
[6] S.M. Park, J.G. Jang, S.A. Chae, H.K. Lee, An NMR spectroscopic investigation of aluminosilicate gel in alkali-activated fly ash in a CO_2-rich environment, Materials 9 (2016) 308.
[7] J.L. Provis, Alkali-activated materials, Cement Concr. Res. 114 (2018) 40–48.
[8] C. Shi, P.V. Krivenko, D.M. Roy, Alkali-activated Cements and Concretes, Taylor & Francis, Abingdon, UK, 2006.
[9] Z. Mazrouei-Sebdani, L. Javazmi, A. Khoddami, F. Shams-Ghahfarokhi, T. Low, Fabrication of a silica aerogel and examination of its hydrophobic properties via contact angle and 3M water repellency tests, IOP Conf. Ser. Mater. Sci. Eng. 204 (2017), 012014.
[10] J. Labudek, L. Martiník, Aerogel-material of the future for civil engineering, Trans. VŠB - Tech. Univ. Ostrava. Const. Series 11 (2011) 1–9.
[11] S.D. Bhagat, K.T. Park, Y.H. Kim, J.S. Kim, J.H. Han, A continuous production process for silica aerogel powders based on sodium silicate by fluidized bed drying of wet-gel slurry, Solid State Sci. 10 (2008) 1113–1116.
[12] R. Baetens, B.P. Jelle, A. Gustavsen, Aerogel insulation for building applications: a state-of-the-art review, Energy Build. 43 (2011) 761–769.
[13] H. Cheng, H. Xue, C. Hong, X. Zhang, Preparation, mechanical, thermal and ablative properties of lightweight needled carbon fibre felt/phenolic resin aerogel composite with a bird's nest structure, Compos. Sci. Technol. 140 (2017) 63–72.
[14] A.C. Pierre, G.M. Pajonk, Chemistry of aerogels and their applications, Chem. Rev. 102 (2002) 4243–4266.
[15] M.Z. Yazdan-Abad, M. Noroozifar, A.R.M. Alam, H. Saravani, Palladium aerogel as a high-performance electrocatalyst for ethanol electro-oxidation in alkaline media, J. Mater. Chem. 5 (2017) 10244–10249.
[16] H. Xuan, J. Ren, X. Wang, J. Zhang, L. Ge, Flame-retardant, non-irritating and self-healing multilayer films with double-network structure, Compos. Sci. Technol. 145 (2017) 15–23.
[17] L. Zuo, W. Fan, Y. Zhang, L. Zhang, W. Gao, Y. Huang, T. Liu, Graphene/montmorillonite hybrid synergistically reinforced polyimide composite aerogels with enhanced flame-retardant performance, Compos. Sci. Technol. 139 (2017) 57–63.
[18] D.Y. Nadargi, A.V. Rao, Methyltriethoxysilane, New precursor for synthesizing silica aerogels, J. Alloy. Comp. 467 (2009) 1–2.
[19] W. Guo, J. Liu, P. Zhang, L. Song, X. Wang, Y. Hu, Multi-functional hydroxyapatite/polyvinyl alcohol composite aerogels with self-cleaning, superior fire resistance and low thermal conductivity, Compos. Sci. Technol. 158 (2018) 128–136.
[20] T. Gao, B.P. Jelle, A. Gustavsen, S. Jacobsen, Aerogel-incorporated concrete: an experimental study, Constr. Build. Mater. 52 (2014) 130–136.
[21] S. Ng, B.P. Jelle, L.I.C. Sandberg, T. Gao, Ó.H. Wallevik, Experimental investigations of aerogel-incorporated ultra-high performance concrete, Constr. Build. Mater. 77 (2015) 307–316.
[22] S. Ng, B.P. Jelle, Y. Zhen, Ó.H. Wallevik, Effect of storage and curing conditions at elevated temperatures on aerogel-incorporated mortar samples based on UHPC recipe, Constr. Build. Mater. 106 (2016) 640–649.
[23] M. de Fátima Júlio, A. Soares, L.M. Ilharco, I. Flores-Colen, J. de Brito, Silica-based aerogels as aggregates for cement-based thermal renders, Cement Concr. Compos. 72 (2016) 309–318.
[24] Y. Huang, L. Gong, Y. Pan, C. Li, T. Zhou, X. Cheng, Facile construction of the aerogel/geopolymer composite with ultra-low thermal conductivity and high mechanical performance, RSC Adv. 8 (2018) 2350–2356.
[25] ASTM C618-19, Standard Specification for Coal Fly Ash and Raw or Calcined Natural Pozzolan for Use in Concrete, ASTM International, West Conshohocken, PA, 2019.
[26] Y.B. Ahn, J.G. Jang, H.K. Lee, Mechanical properties of lightweight concrete made with coal ashes after exposure to elevated temperatures, Cement Concr. Compos. 72 (2016) 27–38.
[27] H.J. Yim, S.J. Park, J.H. Kim, H.G. Kwak, Nonlinear ultrasonic method to evaluate residual mechanical properties of thermally damaged concrete, ACI Mater. 111 (2014) 399.
[28] S.M. Park, J.G. Jang, N.K. Lee, H.K. Lee, Physicochemical properties of binder gel in alkali-activated fly ash/slag exposed to high temperatures, Cement Concr. Res. 89 (2016) 72–79.
[29] A.N. Murri, W.D.A. Rickard, M.C. Bignozzi, A. Van Riessen, High temperature behavior of ambient cured alkali-activated materials based on ladle slag, Cement Concr. Res. 43 (2013) 51–61.
[30] D.L. Kong, J.G. Sanjayan, Effect of elevated temperatures on geopolymer paste, mortar and concrete, Cement Concr. Res. 40 (2010) 334–339.
[31] R. Zhang, X. Cheng, P. Hou, Z. Ye, Influences of nano-TiO_2 on the properties of cement-based materials: hydration and drying shrinkage, Constr. Build. Mater. 81 (2015) 35–41.
[32] K. Zheng, L. Chen, M. Gbozee, Thermal stability of geopolymers used as supporting materials for TiO2 film coating through sol-gel process: feasibility and improvement, Constr. Build. Mater. 125 (2016) 1114–1126.
[33] Q. Zeng, K. Li, T. Fen-Chong, P. Dangla, Effect of porosity on thermal expansion coefficient of cement pastes and mortars, Constr. Build. Mater. 28 (2012) 468–475.
[34] W.D. Rickard, A.V. Riessen, P. Walls, Thermal character of geopolymers synthesized from class F fly ash containing high concentrations of iron and α-quartz, Int. J. Appl. Ceram. Technol. 7 (2010) 81–88.
[35] P.R.L. Welche, V. Heine, M.T. Dove, Negative thermal expansion in beta-quartz, Phys. Chem. Miner. 26 (1998) 63–77.
[36] J.L. Provis, R.M. Harrex, S.A. Bernal, P. Duxson, J.S. van Deventer, Dilatometry of geopolymers as a means of selecting desirable fly ash sources, J. Non-Cryst. Solids 358 (2012) 1930–1937.
[37] D. Kubatová, A. Rybová, A. Zezulová, J. Švec, Thermal behavior of inorganic aluminosilicate polymer based on cement kiln dust, IOP Conf. Ser. Mater. Sci. Eng. 379 (2018), 012008.
[38] N. Abbas, H.R. Khalid, G. Ban, H.T. Kim, H.K. Lee, Silica aerogel derived from rice husk: an aggregate replacer for lightweight and thermally insulating cement-based composites, Constr. Build. Mater. 195 (2019) 312–322.
[39] H.M. Son, S.M. Park, J.H. Seo, H.K. Lee, Effect of $CaSO_4$ incorporation on pore structure and drying shrinkage of alkali-activated binders, Materials 12 (2019) 1673.
[40] O. Tsioulou, J. Erpelding, A. Lampropoulos, Development of Novel Low Thermal Conductivity Concrete Using Aerogel Powder, 2016.
[41] J. Strzałkowski, H. Garbalińska, Thermal and strength properties of lightweight concretes with the addition of aerogel particles, Adv. Cem. Res. 28 (2016) 567–575.
[42] P. Duxson, G.C. Lukey, J.S. van Deventer, Physical evolution of Na-geopolymer derived from metakaolin up to 1000 °C, J. Mater. Sci. 42 (2007) 3044–3054.
[43] M.G. Gomes, I. Flores-Colen, L.M. Manga, A. Soares, J. be Brito, The influence of moisture content on the thermal conductivity of external thermal mortars, Construct. Build. Mater. (2017).
[44] Y. Wu, J.Y. Wang, P.J. Moteiro, M.H. Zhang, Development of ultra-lightweight cement composites with low thermal conductivity and high specific strength for energy efficient buildings, Construct. Build. Mater. (2015) 100–112.

[45] I. Ismail, S.A. Bernal, J.L. Provis, V. Rose, R.M. Gutierrez, Evolution of binder structure in sodium silicate-activated slag-metakaolin blends, Cement. Concrete. Composites. (2011) 46–54.
[46] N.K. Lee, J.G. Jang, H.K. Lee, Shrinkage characteristics of alkali-activated fly ash/slag paste and mortar at early ages, Cement. Concrete. Composites. (2014) 239–248.
[47] J.G. Jang, N.K. Lee, H.K. Lee, Fresh and hardened properties of alkali-activated fly ash/slag pastes with superplasticizers, Construc. Build. Mater. (2014) 169–176.
[48] S.A. Bernal, R.M. Gutierrez, F. Ruiz, H. Quinones, J.L. Provis, High-temperature performance of mortars and concretes based on alkaliactivated slag/metakaolin blends, Materiales de Construcción (2012) 471–488.
[49] S.A. Bernal, E.D. Rodriguez, R.M. Gutierrez, M. Gordillo, J.L. Provis, Mechanical and thermal characterisation of geopolymers based on silicate-activated metakaolin/slag blends, J. Mater. Sci. (2011) 5477–5486.
[50] E. Kapeluszna, Ł. Kotwica, A. Różycka, Ł. Gołek, Incorporation of Al in CASH gels with various Ca/Si and Al/Si ratio: Microstructural and structural characteristics with DTA/TG, XRD, FTIR and TEM analysis, Construct. Build. Mater. (2017) 643–653.